

Journal of Materials Chemistry A

Accepted Manuscript



This is an *Accepted Manuscript*, which has been through the Royal Society of Chemistry peer review process and has been accepted for publication.

Accepted Manuscripts are published online shortly after acceptance, before technical editing, formatting and proof reading. Using this free service, authors can make their results available to the community, in citable form, before we publish the edited article. We will replace this *Accepted Manuscript* with the edited and formatted *Advance Article* as soon as it is available.

You can find more information about *Accepted Manuscripts* in the [Information for Authors](#).

Please note that technical editing may introduce minor changes to the text and/or graphics, which may alter content. The journal's standard [Terms & Conditions](#) and the [Ethical guidelines](#) still apply. In no event shall the Royal Society of Chemistry be held responsible for any errors or omissions in this *Accepted Manuscript* or any consequences arising from the use of any information it contains.

ARTICLE

A Triple-layered, Hierarchical 1D Core-shell Nanostructure with a Plasmonic Ag Octahedra Core for Use in Solid-state Dye-sensitized Solar Cells

Cite this: DOI: 10.1039/x0xx00000x

Dong Jun Kim,^a Sung Hoon Ahn,^b Chang Soo Lee,^a Jong Hak Kim^{*a}Received 00th January 2012,
Accepted 00th January 2012

DOI: 10.1039/x0xx00000x

www.rsc.org/

A triple-layered, core-shell nanostructure is prepared with a Ag octahedra, SnO₂ nanotube (SNT), and TiO₂ nanosheet (TNS) via a combined process of electrospinning and solvothermal reaction. In particular, a facile one-step synthesis process for Ag octahedra nanocrystals is suggested. The Ag@SNT@TNS hetero-nanostructure is uniformly distributed in organized TiO₂ film derived with poly(vinyl chloride)-graft-poly(oxyethylene methacrylate) (PVC-g-POEM) graft copolymer and hydrophilically-pretreated TiO₂ nanocrystals. The efficiency of the solid-state dye-sensitized solar cells (ssDSSCs) fabricated with this hetero-nanostructure reaches 7.8% at 100 mW cm⁻², which is much greater than that of cells without a hetero-nanostructure (5.2%) or that prepared with commercially-available Dyesol paste (4.4%). This higher efficiency is attributed to the one-dimensional (1D) tubular structure, the improved surface area, and the plasmonic effect of Ag octahedra nanocrystals, resulting in enhanced short-circuit current density (J_{sc}), as confirmed by the incident photon-to-current efficiency (IPCE), electrochemical impedance spectroscopy (EIS), and intensity modulated photocurrent/voltage spectroscopy (IMPS/IMVS).

Introduction

Since 1991, dye-sensitized solar cells (DSSCs) have attracted a lot of interest due to their high cost effectiveness.¹ When the dyes absorb incident light, excited electrons can be transferred to a wide band-gap metal oxide, such as TiO₂, SnO₂ or ZnO, and then vacancies in the dyes are generated by electrons carried in electrolyte from the counter electrode. There are several methods to enhance the performance of DSSCs including modification of the photoanodes,²⁻⁴ dye structure⁵ and electrolytes.^{6,7} A critical factor is the charge collection that is related to the amount of dye adsorption and extended the wavelength absorbed. Many research groups have tried to enhance the charge collection using the light trapping layer,⁸⁻¹⁰ co-sensitization,¹¹ and plasmonic nanoparticles.^{12,13} Recently, solar cells with organic-inorganic hybrid perovskite showed higher efficiency due to the use of a narrow band gap material, 'CH₃NH₃PbI₃', that can absorb most of the visible range of the spectrum.^{14,15}

Although many noble metals have been considered valuable materials, their nanoparticle forms have attracted more interest due to special properties such as catalytic activity and localized surface plasmon resonance (LSPR).¹⁶ The LSPR phenomenon is induced by collective oscillation of electrons, so when the light is incident to the noble metal nanoparticles, such as Ag or Au, the visible light is simultaneously absorbed and scattered. Furthermore, the absorption spectrum strongly depends on the size, shape and other attributes of

the particles.^{17,18} Because of the observed extinction property (absorption + scattering), plasmonic nanoparticles have often been used in solar cells¹⁹⁻²¹ or photocatalysts to enhance performance. Particularly, in solar cells, two different positive effects, the charging effect and plasmonic effect, have been confirmed by many investigations.²²⁻²⁴ The charging effect causes the fermi-level of the semiconductor to negatively-shift favorably to the open circuit voltage (V_{oc}), and the plasmonic effect enhances the light absorption related to the short-circuit current density (J_{sc}) by extending the light path.²⁵

Despite a high efficiency up to 12.3% for DSSCs based on a liquid electrolyte, the long-term stability of the device requires adequate sealing techniques to prevent leakage and evaporation of the liquid. This challenge is important, especially for outdoor applications. To address this issue, solid-state dye-sensitized solar cells (ssDSSCs) based on hole transport materials or solid polymer electrolytes have been considered as alternatives to liquid electrolyte-based DSSCs.^{10,26-30} In our previous work, we fabricated ssDSSCs with a 7.1% efficiency based on crack-free, organized mesoporous TiO₂ film using poly(vinyl chloride)-graft-poly(oxyethylene methacrylate) (PVC-g-POEM) graft copolymer as a structure directing agent.²⁹ Additionally, we recently reported a one-dimensional (1D) hierarchical structure dispersed in organized mesoporous TiO₂ film, resulting in increased efficiency due to the enhanced surface area, electron transport and scattering effect.³⁰

In this study, we report ssDSSCs with an improved efficiency up to 7.8% at 100 mW cm⁻² based on the triple-layered core-shell hetero-nanostructure. We highlight a facile one-step synthesis method of Ag octahedral nanocrystals via a polyol process and the plasmonic effect of the Ag octahedra, an organized TiO₂ film, and a hierarchical 1D structure on the performance of ssDSSCs. Electrospinning was used to embed Ag nanocrystals in a SnO₂ nanotube (SNT), while a TiO₂ nanosheet (TNS) was deposited on the surface of the Ag@SNT (AS) structure via a solvothermal process. As a result, a triple-layered core-shell structure, Ag@SNT@TNS (AST), was prepared, and hetero-nanostructures were inserted to the organized TiO₂ film. The structures were characterized with normal and back-scattering modes of a field emission scanning electron microscope (FE-SEM). We fabricated a series of ssDSSCs according to the amount of added Ag nanocrystals and investigated performances with current density-voltage (J-V) curves, electrochemical impedance spectroscopy (EIS) spectra, incident photon-to-current efficiency (IPCE) spectroscopy, intensity-modulated photocurrent spectroscopy (IMPS) and intensity-modulated photovoltage spectroscopy (IMVS).

Experimental section

Materials

Silver trifluoroacetate (AgCF₃COO, 98%), sodium hydrosulfide hydrate (NaSH), poly(vinyl pyrrolidone) (PVP, M_w = 55,000 g/mol, M_v = 1.3M g/mol), ethylene glycol (EG, anhydrous, 99.8%), hydrochloric acid (ACS reagent, 37%), titanium isopropoxide (TTIP, 97%), diethylenetriamine (DETA, 99%) and tin chloride (SnCl₂, 98%) were purchased from Sigma Aldrich. Absolute ethanol, N,N-dimethylformamide (DMF), tetrahydrofuran (THF), acetone and isopropanol (IPA) were purchased from J.T. Baker. All the chemicals were used without further purification.

Synthesis of silver (Ag) octahedra nanocrystals

First, 30 ml of EG was put into a 500 ml round-bottom flask and maintained at 150°C for 30 min to eliminate residual water. Then, 0.5 g of PVP (M_w = 55,000 g mol⁻¹) was dissolved in 25 ml of EG, and 0.248 g of AgCF₃COO was separately dissolved in 4 ml of EG. At 150°C, 1 ml of a NaSH solution (3mM) and HCl (3mM) in EG were separately added to the round-bottom flask; between the additions, the solution was maintained for 2 min at temperature. Next, 8 ml of PVP solution was added to the round-bottom flask and maintained for 2 min. Finally, 2.4 ml of the AgCF₃COO solution was very slowly added to the solution with a syringe and maintained for 1 h. After the reaction was complete, the product was precipitated in acetone via centrifugation and washed several times with ethanol to eliminate the residual PVP. The final product was re-distributed in 10 ml of ethanol, and 1 g of PVP (M_v = 1.3M g mol⁻¹) was dissolved in the colloid to stabilize the Ag nanocrystals.

Embedding the Ag octahedral in the SnO₂ nanotube for preparation of Ag@SNT (AS)

For AS0 (without Ag), 0.4 g of SnCl₂ was dissolved in a 1:1 mixture of DMF and ethanol for 1 h at room temperature, and then 0.5 g of PVP (M_v = 1.3M g mol⁻¹) was dissolved in a prepared solution for 3 h at room temperature. The solution was electrospun with 0.5 ml h⁻¹ and 15 kV, and collected at a temperature of 80°C, and then the electrospun product was maintained in an oven to evaporate the residual solvents at 120°C for 12 h. Finally, the product was calcined to eliminate PVP and anneal SnO₂ at 500°C for 1 h. For AS1, 2 and 3, 0.5 ml, 1 ml, 1.5 ml respectively of the Ag colloid with an equal amount of ethanol up to a solution volume of 2.5 ml and 2.5 ml of DMF were used as the solution. The rest of the processes were repeated with the same method as for the synthesis of AS0.

Surface-modification with TiO₂ nanosheets for preparation of Ag@SNT@TNS (AST)

For surface modification with the TiO₂ nanosheets (TNS), 0.5 g of each AS series sample were distributed in 40 ml of IPA with vigorous stirring and sonication. Then, 0.3 ml of DEAT and 0.3 ml of TTIP were added to the IPA solution. The solution was transferred to a 100 ml Teflon-lined autoclave and maintained in an oven at 200°C for 24 h. The product at the bottom of the autoclave was carefully retrieved, dried, and calcined at 450°C for 30 min.

Preparation of photoanodes

For the preparation of the organized TiO₂ (OT) film used as a reference, the hydrophilically pre-treated, preformed TiO₂ nanocrystals and poly(vinyl chloride)-graft-poly(oxyethylene methacrylate) (PVC-g-POEM) solution in THF was used according to a previous work. To this, 15 ml of HCl (37%) was slowly added to induce self-assembly of the graft copolymer and to increase dispersion of the hydrophilically-pretreated TiO₂ nanocrystals. For the AST series, 0.03 g of AST0-3 was added before dissolution of the copolymer and stirred for a day to achieve adequate distribution; the rest of the processes were the same. Finally, each viscous solution was cast onto a 20-nm blocking layer-coated FTO glass with a doctor blade method and calcined at 450°C for 30 min.

Fabrication of ssDSSCs

The above OT and AST series were used as photoanodes with an active area of 0.16 cm², and the photoanodes were sensitized with an N719 dye solution in ethanol (10⁻⁴M) at 50°C for 3 h. To prepare the counter electrode, a 4% solution of H₂PtCl₆ in IPA was spin-coated onto bare FTO glass and calcined at 450°C for 30 min. A solid powder, poly((1-(4-ethenylphenyl)methyl)-3-butyl-imidazolium iodide) (PEBII, M_w = 15 000 g mol⁻¹), was synthesized by three-step reaction and used as a solid electrolyte.^{29,30,38} The PEBII solution in acetonitrile was directly cast onto the photoanodes. The photoanodes and counter electrodes were then superimposed and pressed between two glass plates to achieve slow solvent evaporation and create a thin electrolyte layer. The cells were placed in a vacuum oven for one day to ensure complete solvent evaporation. The cells were sealed with an epoxy resin. More than six identical devices were fabricated and tested. The average estimated error of efficiency was approximately ± 5%.”

Characterization

The film morphologies were characterized with a field-emission scanning electron microscope (FE-SEM, SUPRA 55VP, Carl Zeiss, Germany & JSM-7001F, JEOL, Japan). Absorbance of the Ag colloid and reflectance of the TiO₂ films were measured by UV-Vis spectroscopy (Lambda 750, Perkin Elmer, USA). The photo-electrochemical performance of the ssDSSCs was characterized by an electrochemical workstation (Keithley Model 2400) and a solar simulator (1000 W xenon lamp, Oriel, 91193) whose light was homogeneous across an 8 × 8 area and was calibrated with a Si solar cell (Fraunhofer Institute for Solar Energy System, Mono-Si+KG filter, Certificate No. C-ISE269) to an intensity of 1 sun (100 mW cm⁻²). Electrochemical impedance spectroscopy (EIS) was performed with a CompactStat electrochemistry analyzer (IVIUM Technologies) with frequencies ranging from 100 kHz to 0.05 Hz and a potential modulation of 0.02 V under AM 1.5 (at 100 mW cm⁻²) light illumination. Incident photon-to-current efficiency (IPCE) was measured over wavelengths ranging from 300 to 800 nm using a 150 W Arc Xe lamp source (K3100, McScience). Intensity-modulated photocurrent/voltage spectroscopy (IMPS/IMVS) spectra were measured with a frequency response analyzer under a modulated red light emitting diode (635 nm).

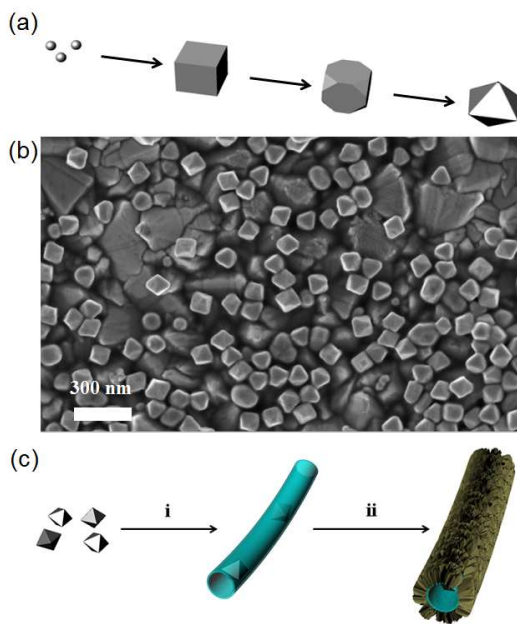


Fig. 1 (a) Schematic illustration of the synthesis of a Ag octahedron, (b) FE-SEM image of a Ag octahedron on fluorine-doped tin oxide (FTO) glass, (c) schematic explanation of the synthesis of the triple-layered core-shell structure, i.e., Ag@SNT@TNS (AST) series: i) electrospinning with a mixture of Ag octahedra and SnCl₂ solution to form Ag@SNT, ii) solvothermally-grown TiO₂ nanosheets (TNS) on the Ag@SNT to form Ag@SNT@TNS.

Results and Discussion

The characteristic optical signature for octahedral-shaped nanocrystals has a much greater complexity than the other polyhedral shapes, and octahedral nanocrystals exhibit several strong LSPR modes and a fine structure in the form of less intense resonances.³¹ Thus, we synthesized silver octahedron nanocrystals with a 90-100 nm size and a regular shape bound entirely by {100} and {111} facets of the face centered cubic (FCC) crystal lattice, as shown in Fig. 1a,b. We suggest a facile one-step synthetic procedure by modifying the methods developed by two independent groups, i.e., the Yang group³¹ and the Xia group.^{32,33} The Yang group used AgNO₃ as a silver precursor for transition of the crystalline structure from the Ag cube to the Ag octahedron with the simultaneous extinction and creation of the {100} and {111} planes. However, the use of AgNO₃ involves the emission of a toxic nitrogen gas during the polyol process; thus, the Xia group adopted AgCF₃COO as an alternative precursor. Silver nanocubes with various sizes were synthesized, but silver octahedra could not be synthesized.³² Later, the Xia group synthesized silver octahedra with edge lengths in the range of 20-72 nm via a two-step, seed-mediated growth approach.³³

In our study, we describe a facile, one-step method for the synthesis of silver octahedra nanocrystals based on the careful control of the amount of AgCF₃COO as a safe silver precursor. A larger amount of the silver precursor lead to the transition to Ag octahedrons with regular hexagonal faces, which is the optimal particle shape for an FCC metal based on energy considerations. As shown in Fig. S1, Ag nanocrystals with a cube structure were formed when synthesizing with insufficient reactants and a shorter reaction time, indicating that octahedra are the most likely structure in a complete reaction. Initially, small silver nanocrystals nucleate and develop into nanocubes bound by {100} planes³⁴, which are selectively stabilized by adsorbed hydrophilic long chain molecules such as poly(vinyl pyrrolidone) (PVP). With time, silver deposits selectively onto the {100} nanocrystal facets, and the {111}-capped corners of the nanocube are stabilized. Finally, the nanocrystal evolves from a {100}-bound cube to a {111}-bound octahedron.³¹

The synthesized Ag octahedral nanocrystals were adopted as plasmonic nanoparticles in a triple layered, core-shell hetero-nanostructure for ssDSSC applications, as shown in Fig. 1c. First, the Ag octahedral colloid was electrospun with a SnCl₂ precursor solution containing hydrophilic PVP to form Ag@SnO₂ nanotubes (Ag@SNT) upon calcination at 500 °C. The Ag octahedra nanocrystals were not used in the AS0 sample, while the amount of Ag octahedra increased from AS1 to AS3. The amounts of total solvent and PVP were fixed. As shown in Fig. 2a, b, the 1D tubular structure with a diameter of 200-300 nm was prepared, regardless of whether or not Ag octahedra were used, indicating the negligible effect of Ag nanocrystals for the formation of a SnO₂ nanotube structure. When comparing AS0 and AS2, the existence of Ag nanocrystals in the SNT was confirmed with back-scattering mode of FE-SEM, as shown in Fig. 2c, d, and the amount of Ag nanoparticles increased from AS1 to AS3 (Fig. S2). In order to modify the Ag@SNT surface with TiO₂ nanosheets (TNS), diethylenetriamine (DETA) and titanium isopropoxide (TTIP) were

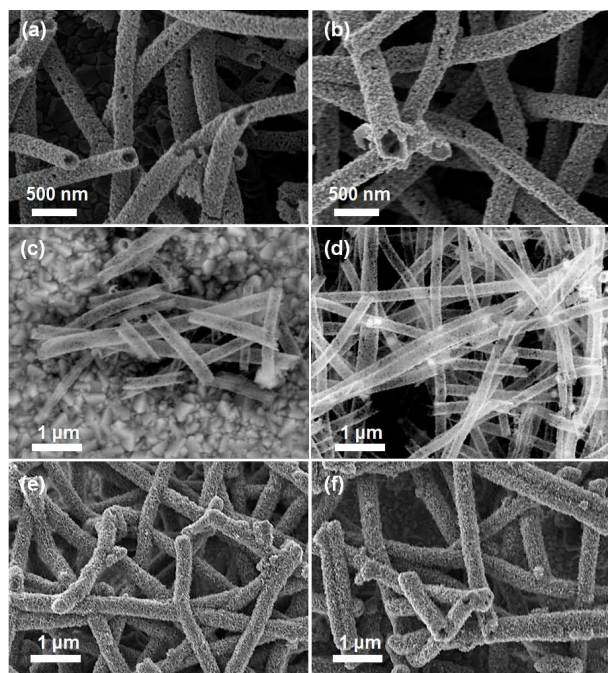


Fig. 2 FE-SEM images of (a) AS0, (b) AS2, (c) AS0 (back-scattering mode), (d) AS2 (back-scattering mode), (e) AST0, and (f) AST2.

used as a structure controlling agent and TiO_2 precursor, respectively. Upon the solvothermal reaction at 200°C for 24 h, a triple-layered, core-shell hetero-nanostructure ($\text{Ag}@\text{SNT}@\text{TNS}$) was formed, as confirmed by FE-SEM in Fig. 2e, f. The TNS decorated the outer side as well as inside of the SNT and thus the surface modification of SNT by TNS led to the increased surface area from 73.9 to $85.8 \text{ cm}^2/\text{g}$.³⁰

Next, a series of photoanodes was prepared on the blocking-layered, fluorine-doped tin oxide (FTO) glass via a one-step, doctor-blade method using organized TiO_2 (OT) film as a matrix to disperse the core-shell hetero-nanostructure. The OT film was prepared via self-assembly of the hydrophilic-pretreated TiO_2 nanocrystals and the PVC-g-POEM graft copolymer.²⁹ As shown in Fig. 3a,b, the OT film with an approximate $10 \mu\text{m}$ thickness exhibited a well-organized mesostructure with large pores ($\sim 50 \text{ nm}$), high porosity and good interconnectivity. The PVC-g-POEM graft copolymer is effective in templating organized TiO_2 mesostructures into the hydrophilic rubbery POEM side chains and the hydrophobic glassy PVC main chains due to its high molecular weight ($1.1 \times 10^5 \text{ g/mol}$) and well-defined, microphase-separated morphology.³⁵ The hydrophilically-pretreated TiO_2 nanocrystals play an important role as a structural binder for maintaining an organized structure without crack formation at $10 \mu\text{m}$ thickness. The hydrophilically-pretreated TiO_2 nanocrystals have preferential interactions with the hydrophilic rubbery POEM side chains, which are responsible for the well-ordered mesostructure of the OT film. The amount of Ag octahedral nanocrystals was systematically increased from AST0 to AST3 (Table 1). The AST hetero-nanostructures were well embedded and uniformly dispersed in the OT film without large interfacial

boundaries, as shown in Fig. 3c-f. The crystalline structure of Ag, SnO_2 and TiO_2 was confirmed by X-ray diffraction (XRD), as shown in Fig. S3. The organized mesostructures of the OT film were maintained and homogenized with the triple-layered, core-shell hetero-nanostructure, indicating good interfacial contact between the nanostructures and the matrix. The relatively low density of the hetero-nanostructure due to the high porosity and empty voids inside the shell helped to facilitate the uniform distribution.

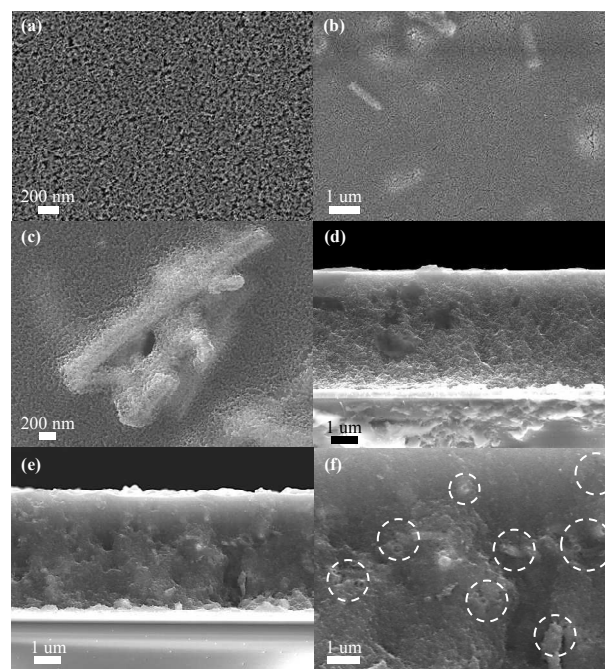


Fig. 3 FE-SEM images of the (a) surface and (b) cross-section of OT film, (c) (d) surface of AST2 film, and (e) (f) cross-section of AST2 film. The AST hetero-nanostructure is marked with white circles.

In order to investigate the improvement in optical properties caused by the plasmonic effect, the UV-Vis absorbance and reflectance of the Ag octahedra and TiO_2 films were measured as in Fig. 4a. A broad peak with plasmonic absorption and scattering was observed for the Ag octahedra, which is strong support for the formation of the octahedral nanostructure rather than a sphere-like or cube structure.^{34,36,37} The morphology of Ag octahedra was hardly changed even after the thermal treatment although some of edges were very little smoothed.³⁷ The reflectance of the OT film was the lowest due to its high transparency. The AST series showed greater reflectance, indicating 1) a scattering effect of the 1D structure and 2) plasmonic absorption and scattering. The former was confirmed by the difference between OT and AST0, while the latter was confirmed by the differences among the AST series members. Additionally, the slight reflectance band near 500 nm for the AST series is another indicator of plasmonic absorption. The absorption spectra of dyes detached from each photoanode in NaOH solution in a mixture of ethanol and H_2O were characterized as shown in Fig. 4b. The amount of dye loading was calculated and is specified in Table 1. The dye loadings were not significantly different among the

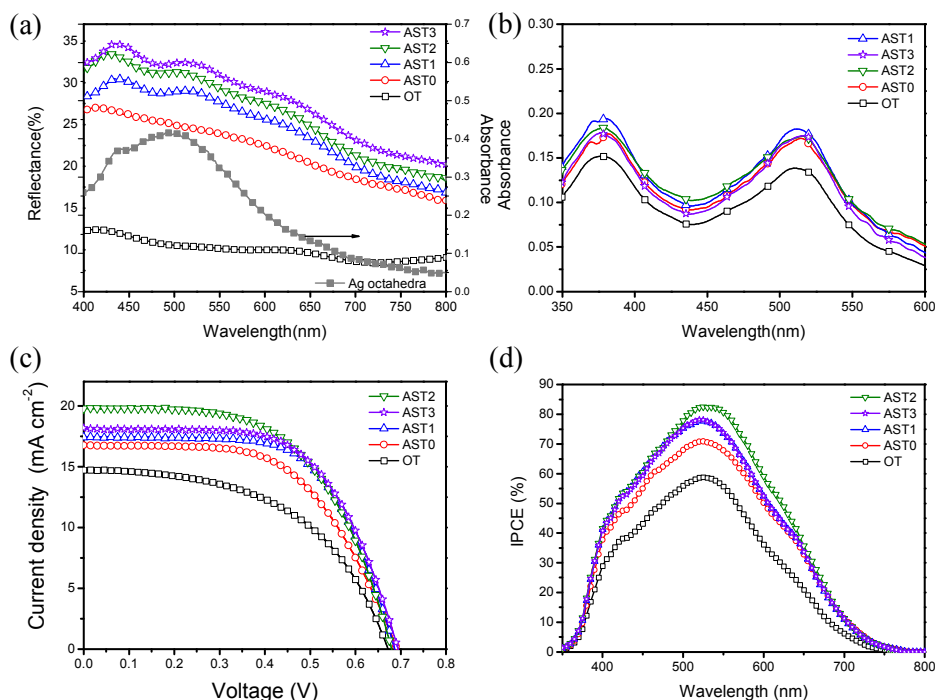


Fig. 4 (a) UV-Vis spectra of the Ag octahedra and reflectance of various photoanodes, (b) dye solution detached from the photoanodes, (c) J-V curves and (d) IPCE spectra of ssDSSCs fabricated with a 10- μm -thick photoanode and a solid PEBII electrolyte under 1 sun (at 100 mW cm^{-2}).

AST series photoanodes but were much greater than that of the OT photoanode. The TNS plays an important role in improving the surface area of the photoanode due to the {001} facet of TNS, which is favorable for increasing the dye loading.³⁰

The ssDSSCs were fabricated with various photoanodes, a thermal-annealed Pt counter electrode and solid electrolyte, i.e., poly((1-(4-ethenylphenyl)methyl)-3-butyl-imidazolium iodide) (PEBII). The PEBII is a single-component solid electrolyte with good stability and high ionic conductivity, without any need for additives such as iodine (I_2) or iodide salts.^{29,38} The high conductivity results from flexible rubbery chains and a well-organized structure achieved through π - π stacking interactions. The current density-voltage (J-V) curves measured at 100 mW cm^{-2} were plotted in Fig. 4c, and V_{oc} , J_{sc} and fill factor (FF) are specified in Table 1. The OT photoanode prepared by the self-assembly of hydrophilically-pretreated TiO_2 nanocrystals and the PVC-g-POEM graft copolymer is more advantageous than randomly-organized TiO_2 (RT) film due to the larger surface area, higher porosity and better interconnectivity between ordered blocks. As a result, the conversion efficiency of the OT-based ssDSSC (5.2 %) was greater than that of the RT-based cell (4.4 %) prepared with commercially-available paste (Dyesol 18NR-T) due to higher V_{oc} and J_{sc} values. This demonstrates that photoanodes with a well-organized mesostructure play a pivotal role in improving the efficiency of ssDSSCs. All hybrid systems consisting of AST hetero-nanostructures dispersed in the OT matrix showed improved energy conversion efficiency compared to the neat OT-based cell. The AST0 showed an efficiency of 6.6 % with higher J_{sc} value due to

increased dye loading, greater light scattering, and enhanced electron transport, as well as higher FF value attributed to better pore-filling of electrolyte. The efficiency consistently increased from AST0 to AST2 with the amount of AST in the photoanode. The highest efficiency reaching 7.8% was obtained at 100 mW/cm^2 for the AST2 cell, which is among the highest values observed for the N719-based ssDSSCs^{28-30,38-45} and is 1.8-fold greater than that of the commercially-available TiO_2 . The obtained cell efficiency was not significantly changed at room temperature up to 200 h. The increased FF value of the AST series compared to the OT-based cell can be explained by better solid electrolyte infiltration caused by the 1D hetero-nanostructure with the high porosity and empty voids inside the shell, as confirmed by the above FE-SEM image. The increase in J_{sc} value from AST0 to AST2 is attributed to the plasmonic effect of the Ag octahedra because all the other factors were fixed except for the Ag amount. This increasing tendency in J_{sc} values was repeatedly confirmed by IPCE spectra, as shown in Fig. 4d. In other words, the J_{sc} increase in the range of 600-700 nm, a relative longer wavelength, is due to the scattering of the Ag octahedra and 1D tubular structures, while the increase at relatively shorter wavelengths is attributed to plasmonic light trapping.^{20,41} A slight difference in J_{sc} values obtained from J-V curves and IPCE spectra might be due to the fact that the large molecular volume solid electrolyte has a low diffusion coefficient and photo-response.⁴⁶ Thus, our ssDSSCs might not have reached the steady-state due to the relatively short incident time for each wavelength during IPCE measurements.

Table 1. Dye loading of photoanodes and photovoltaic performance and electrochemical property of ssDSSCs fabricated with a 10- μm -thick photoanode and a solid PEBII electrolyte.

Photoanode ⁺	V _{oc} (V)	J _{sc} ⁺⁺ (mA cm ⁻²)	FF	Efficiency (%)	Dye loading (nmol cm ⁻²)	R ₃ (Ω)
OT	0.67	14.8 (12.3)	0.52	5.2	157.3	21.7
AST0	0.69	16.8 (16.1)	0.57	6.6	199.8	10.6
AST1	0.69	17.5 (17.4)	0.60	7.2	203.4	11.5
AST2	0.68	19.8 (18.4)	0.58	7.8	199.0	23.9
AST3	0.69	18.2 (17.3)	0.59	7.4	196.9	23.1
RT	0.65	13.3	0.51	4.4	106.3	-

⁺OT: organized TiO₂ film prepared using PVC-g-POEM graft copolymer as a template without Ag@SNT@TNS. AST: Ag@SNT@TNS series, i.e., AST0 was prepared using 0.5 g PVP, 0.4g SnCl₂, 0 ml Ag solution, 2.5 ml ethanol and 2.5 ml DMF. AST1 was prepared using 0.45 g PVP, 0.4g SnCl₂, 0.5 ml Ag solution, 2.0 ml ethanol and 2.5 ml DMF. AST2 was prepared using 0.40 g PVP, 0.4 g SnCl₂, 1.0 ml Ag solution, 1.5 ml ethanol and 2.5 ml DMF. AST3 was prepared using 0.35 g PVP, 0.4g SnCl₂, 1.5 ml Ag solution, 1.0 ml ethanol and 2.5 ml DMF. RT: randomly-organized TiO₂ film prepared using commercially-available Dyesol paste (18NR-T).

⁺⁺ values in parenthesis refer to the J_{sc} obtained from IPCE curves.

However, the AST3-based ssDSSC showed inferior performance to the AST2 despite a larger amount of Ag octahera in the photoanode. When the noble metal nanocrystals are applied in DSSCs, they act as recombination sites if they are used directly without surface-modification.^{47,48} In our study, although the Ag octahera nanocrystals were surface-modified with SNT and TNS, the ends of some tubes might not have been completely blocked, thus allowing formation of

recombination sites. Thus, the decreased efficiency of AST3-based ssDSSC might result from increased recombination sites. We investigated the J-V curves under the dark condition, which is the simplest method to determine the relative amount of recombination sites, as plotted in Fig. 5a. As expected, the dark current became greater as the Ag octahera increased from AST0 to AST3. Furthermore, the EIS spectra were measured as shown in Fig. 5b, and the R₁, R₂, and R₃ values were calculated

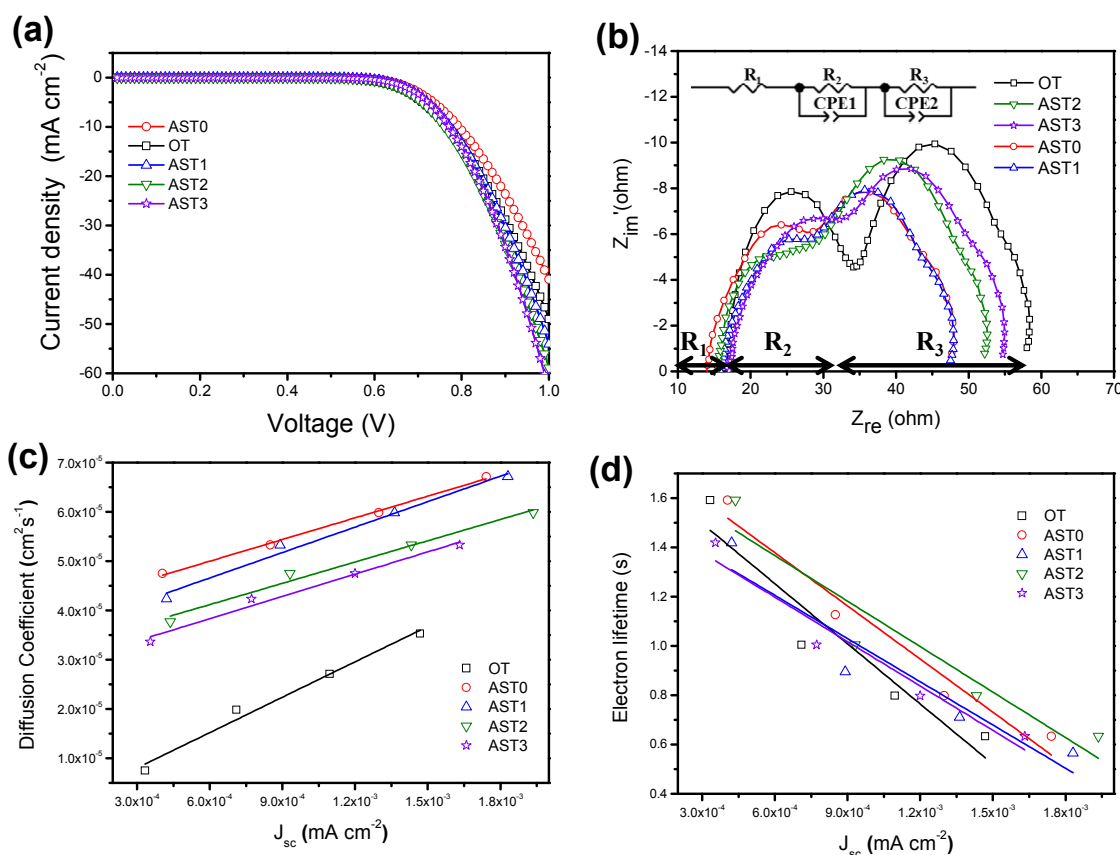


Fig. 5 (a) J-V curves measured under dark conditions, (b) EIS spectra under 1 sun (and equivalent circuit), (c) diffusion coefficient spectra and (d) electron lifetime of ssDSSCs determined from IMPS measurements.

according to the circuit model. Here, R_1 is related to the sheet resistance of the electrodes, R_2 is related to the resistance between the electrolyte and counter electrode, and R_3 is related to the photoanode, dyes, and electrolyte.^{49,50} Because the photoanode was the only variable in this study, the R_3 value was the focus. As shown in Table 1, the R_3 value increased from AST0 to AST3. In particular, the difference between AST1 and AST2 was significant, while the difference between AST2 and AST3 was not notable. In addition, the diffusion coefficients of the ssDSSCs were characterized by IMVS and are plotted in Fig. 5c. Although, the diffusivities of the AST series were greater than that of the OT-based cell, the values decreased from AST0 to AST3, while the electron lifetimes among them were not significantly different (Fig. 5d). Linear regressions of the plots were obtained with the R-square values of over 0.85. Because the same weight of AST0–3 was added to each photoanode, the absolute number of AST decreased from AST0 to AST3 due to the weight of the Ag octahedra. Specifically, the decrease in the number of 1D tubular structures led to a gradual decrease in diffusivity. Conclusively, the efficiency was determined among the AST series members with both positive effects such as plasmonic light trapping and scattering and negative effects such as recombination and decrease in 1D structures. As a result, the highest efficiency was obtained for the AST2-based ssDSSC.

Conclusions

We demonstrated a facile, one-step method for the synthesis of Ag octahedra nanocrystals based on careful control of the amount of AgCF_3COO as a safe silver precursor. Various amounts of Ag octahedra were combined with SnO_2 precursor solution, followed by electrospinning to form a core-shell 1D nanostructure, i.e., Ag@SNT (AS). Surface modification of the TiO_2 nanosheet (TNS) was performed to increase the surface area of the {001} facet via solvothermal reaction with the TTIP and DETA, resulting in formation of a triple-layered, core-shell hetero-nanostructure, i.e., Ag@SNT@TNS (AST). The AST nanostructures were embedded and well dispersed in an organized TiO_2 matrix with large pores, high porosity and good interconnectivity due to their relatively low density resulting from high porosity and empty voids inside the shell. The ssDSSC fabricated with the AST2 photoanode showed the highest efficiency, 7.8 % at 100 mW cm^{-2} , which is among the highest values reported for ssDSSCs based on N719 dye and is 1.8-fold greater than that of the commercially-available TiO_2 . The efficiency enhancement was attributed to an increase in J_{sc} value caused by 1) plasmonic light trapping and scattering of the Ag octahedra, 2) electron transport and scattering with a 1D structure and 3) effective pore filling of solid electrolyte, as characterized by J-V curves, IPCE, EIS and IMPS/IMVS measurements.

Acknowledgements

This work was supported by the Active Polymer Center for Pattern

Integration (2007-0056091), the Center for Advanced Meta-Materials (CAMM) (2014M3A6B3063716) and the Korea Center for Artificial Photosynthesis (KCAP) (2009-0093883).

Notes and references

^a Department of Chemical and Biomolecular Engineering, Yonsei University, 50 Yonsei-ro, Seodaemun-gu, Seoul 120-749, South Korea. E-mail: jonghak@yonsei.ac.kr

^b Department of Mechanical Engineering, Stanford University, Stanford, California 94305, USA.

† Electronic Supplementary Information (ESI) available: [details of any supplementary information available should be included here]. See DOI: 10.1039/b000000x/

- 1 B. O'Regan and M. Grätzel, *Nature*, 1991, **353**, 737–740.
- 2 C.-T. Wu, W.-P. Liao and J.-J. Wu, *J. Mater. Chem.*, 2011, **21**, 2871.
- 3 X. Lü, F. Huang, X. Mou, Y. Wang and F. Xu, *Adv. Mater.*, 2010, **22**, 3719–3722.
- 4 X. Tao, P. Ruan, X. Zhang, H. Sun and X. Zhou, *Nanoscale*, 2015, **7**, 3539–3547.
- 5 J. N. Clifford, E. Martínez-Ferrero, A. Viterisi and E. Palomares, *Chem. Soc. Rev.*, 2011, **40**, 1635.
- 6 D. Högberg, B. Soberats, S. Uchida, M. Yoshio, L. Kloo, H. Segawa and T. Kato, *Chem. Mater.*, 2014, **26**, 6496–6502.
- 7 B. Kim, J. K. Koh, J. Kim, W. S. Chi, J. H. Kim, and E. Kim, *ChemSusChem* 2012, **5**, 2173–2180.
- 8 Z. Hosseini, E. W.-G. Diau, K. Mehrany and N. Taghavinia, *ChemPhysChem*, 2014, **15**, 3791–3799.
- 9 G.-B. Shan and G. P. Demopoulos, *Adv. Mater.*, 2010, **22**, 4373–4377.
- 10 D. J. Kim, J. K. Koh, C. S. Lee and J. H. Kim, *Adv. Energy Mater.*, 2014, **4**, 1400414.
- 11 C.-M. Lan, H.-P. Wu, T.-Y. Pan, C.-W. Chang, W.-S. Chao, C.-T. Chen, C.-L. Wang, C.-Y. Lin and E. W.-G. Diau, *Energy Environ. Sci.*, 2012, **5**, 6460.
- 12 X. Dang, J. Qi, M. T. Klug, P.-Y. Chen, D. S. Yun, N. X. Fang, P. T. Hammond and A. M. Belcher, *Nano Lett.*, 2013, **13**, 637–642.
- 13 M. D. Brown, T. Suteewong, R. S. S. Kumar, V. D'Innocenzo, A. Petrozza, M. M. Lee, U. Wiesner and H. J. Snaith, *Nano Lett.*, 2011, **11**, 438–445.
- 14 N. J. Jeon, J. H. Noh, Y. C. Kim, W. S. Yang, S. Ryu and S. I. Seok, *Nat. Mater.*, 2014, **13**, 897–903.
- 15 A. Mei, X. Li, L. Liu, Z. Ku, T. Liu, Y. Rong, M. Xu, M. Hu, J. Chen, Y. Yang, M. Gratzel and H. Han, *Science*, 2014, **345**, 295–298.
- 16 S. Eustis and M. A. El-Sayed, *Chem. Soc. Rev.*, 2006, **35**, 209–217.
- 17 M. J. Mulvihill, X. Y. Ling, J. Henzie and P. Yang, *J. Am. Chem. Soc.*, 2010, **132**, 268–274.
- 18 W. Niu, L. Zhang and G. Xu, *Nanoscale*, 2013, **5**, 3172–3181.
- 19 H. Dong, Z. Wu, F. Lu, Y. Gao, A. El-Shafei, B. Jiao, S. Ning and X. Hou, *Nano Energy*, 2014, **10**, 181–191.
- 20 R. A. Naphade, M. Tathavadekar, J. P. Jog, S. Agarkar and S. Ogale, *J. Mater. Chem. A*, 2014, **2**, 975–984.
- 21 F. Su, T. Wang, R. Lv, J. Zhang, P. Zhang, J. Lu and J. Gong, *Nanoscale*, 2013, **5**, 9001.
- 22 X. Li, W. C. H. Choy, H. Lu, W. E. I. Sha and A. H. P. Ho, *Adv. Funct. Mater.*, 2013, **23**, 2728–2735.
- 23 O. Amiri, M. Salavati-Niasari and M. Farangi, *Electrochimica Acta*, 2015, **153**, 90–96.
- 24 Y. Wang, J. Zhai and Y. Song, *RSC Adv*, 2015, **5**, 210–214.
- 25 H. Choi, W. T. Chen and P. V. Kamat, *ACS Nano*, 2012, **6**, 4418–4427.
- 26 Y. Bai, Y. Cao, J. Zhang, M. Wang, R. Li, P. Wang, S. M. Zakeeruddin and M. Grätzel, *Nat. Mater.*, 2008, **7**, 626–630.
- 27 S. Powar, T. Daeneke, M. T. Ma, D. Fu, N. W. Duffy, G. Götze, M. Weidelener, A. Mishra, P. Bäuerle, L. Spiccia and U. Bach, *Angew. Chem. Int. Ed.*, 2013, **52**, 602–605.
- 28 T. Stergiopoulos, M. Bidikoudi, V. Likodimos and P. Falaras, *J. Mater. Chem.*, 2012, **22**, 24430–24438.
- 29 S. H. Ahn, W. S. Chi, J. T. Park, J. K. Koh, D. K. Roh and J. H. Kim, *Adv. Mater.*, 2012, **24**, 519–522.

- 30 S. H. Ahn, D. J. Kim, W. S. Chi and J. H. Kim, *Adv. Mater.*, 2013, **25**, 4893–4897.
- 31 A. Tao, P. Sinsersuksakul and P. Yang, *Angew. Chem. Int. Ed.*, 2006, **45**, 4597–4601.
- 32 Q. Zhang, W. Li, L.-P. Wen, J. Chen and Y. Xia, *Chem. - Eur. J.*, 2010, **16**, 10234–10239.
- 33 Y. Wang, D. Wan, S. Xie, X. Xia, C. Z. Huang and Y. Xia, *ACS Nano*, 2013, **7**, 4586–4594.
- 34 Y. Sun, Y. Xia, *Science*, 2002, **298**, 2176–2179.
- 35 D. K. Roh, S. J. Kim, H. Jeon and J. H. Kim, *ACS Appl. Mater. Interfaces*, 2013, **5**, 6615–6621.
- 36 B. J. Wiley, S. H. Im, Z.-Y. Li, J. McLellan, A. Siekkinen and Y. Xia, *J. Phys. Chem. B*, 2006, **110**, 15666–15675.
- 37 W.-L. Liu, F.-C. Lin, Y.-C. Yang, C.-H. Huang, S. Gwo, M. H. Huang and J.-S. Huang, *Nanoscale*, 2013, **5**, 7953–7962.
- 38 W. S. Chi, J. K. Koh, S. H. Ahn, J.-S. Shin, H. Ahn, D. Y. Ryu and J. H. Kim, *Electrochem. Commun.*, 2011, **13**, 1349–1352.
- 39 J. K. Koh, J. Kim, B. Kim, J. H. Kim and E. Kim, *Adv. Mater.*, 2011, **23**, 1641–1646.
- 40 S. Y. Heo, J. K. Koh, G. Kang, S. H. Ahn, W. S. Chi, K. Kim and J. H. Kim, *Adv. Energy Mater.*, 2013, **4**, 1300632.
- 41 F. Lodermeier, R. D. Costa, R. Casillas, F. T. U. Kohler, P. Wasserscheid, M. Prato and D. M. Guldi, *Energy Env. Sci*, 2015, **8**, 241–246.
- 42 H. Wang, J. Li, F. Gong, G. Zhou, and Z. S. Wang, *J. Am. Chem. Soc.*, 2013, **135**, 12627–12633.
- 43 C. Xu, J. Wu, U. V. Desai, D. Gao, *Nano Lett.* 2012, **12**, 2420–2424.
- 44 H. Wang, X. Zhang, F. Gong, G. Zhou, Z.-S. Wang, *Adv. Mater.* 2012, **24**, 121–124.
- 45 W. Zhang, J. Li, S. Jiang, Z. S. Wang, *Chem. Commun.* 2014, **50**, 1685–1687.
- 46 M. Wang, P. Chen, R. Humphry-Baker, S. M. Zakeeruddin, and M. Gratzel, *ChemPhysChem* 2009, **10**, 290–299.
- 47 Y. H. Jang, Y. J. Jang, S. T. Kochuveedu, M. Byun, Z. Lin and D. H. Kim, *Nanoscale*, 2014, **6**, 1823–1832.
- 48 B. Sebo, N. Huang, Y. Liu, Q. Tai, L. Liang, H. Hu, S. Xu and X.-Z. Zhao, *Electrochimica Acta*, 2013, **112**, 458–464.
- 49 N. Yang, J. Zhai, D. Wang, Y. Chen and L. Jiang, *ACS Nano*, 2010, **4**, 887–894.
- 50 D. K. Roh, W. S. Chi, H. Jeon, S. J. Kim and J. H. Kim, *Adv. Funct. Mater.*, 2014, **24**, 379–386.

A triple-layered, core-shell hetero-nanostructure was prepared with Ag octahera, a SnO₂ nanotube (SNT), and a TiO₂ nanosheet (TNS) via a combined process of electrospinning and solvothermal reaction. The resulting solid-state dye-sensitized solar cell showed a 7.8% efficiency, which is much greater than the efficiencies of those without a nanostructure (5.2%) and that prepared with commercially-available Dyesol paste (4.4%). The performance improvement is attributed to a one-dimensional (1D) tubular structure, improved surface area and plasmonic effect of Ag octahedra nanoparticles.

